Studies of resonantly produced plasmas in the H-1NF heliac using a far-infrared scanning interferometer

S. M. Collis,[a] J. Howard, G. B. Warr, C. A. Michael, J. H. Harris, B. D. Blackwell, and D. G. Pretty
Plasma Research Laboratory, Australian National University, Canberra ACT 0200, Australia

(Presented on 8 July 2002)

The H-1NF heliac regularly operates using the ion cyclotron range of frequencies at 0.5 T to produce plasmas with a mixture of hydrogen and helium gases. Due to the complex three-dimensional structure of the magnetic flux surfaces, these plasmas require sophisticated diagnostic systems, with good spatial coverage, to extract meaningful physical information. This article presents a study of the dependence of the plasma density profile on resonant heating conditions and magnetic configuration, using a far-infrared scanning interferometer. Recent modifications to the system and data that illustrate the performance of the interferometer will be discussed. © *2003 American Institute of Physics.* [DOI: 10.1063/1.1538360]

I. INTRODUCTION

The H-1NF[1] is a three-period flexible heliac with a major radius of 1 m and a typical minor radius of 0.2 m. The addition of a helical winding to the poloidal field coil allows access to a variety of magnetic configurations having rotational transforms (ι) varying typically between 1.0 and 2.0.

The H-1NF scanning far-infrared interferometer system[2,3] uses a rotating grating to sweep a probing far-infrared laser beam across the plasma and to provide a frequency offset for heterodyne detection of the plasma-induced phase shift. An overview of the interferometer system, which is configured in a Michelson arrangement, is presented in Sec. II.

We have used the interferometer to study the dependence of the plasma density profile on the magnetic-resonance condition and helical configuration for H/He plasmas produced using ion cyclotron resonant heating at 0.5 T.

II. INTERFEROMETER SYSTEM

Figure 1 shows a Gaussian ray trace of the multiview system[4] with three plasma views installed. The support structure for the internal mirrors is connected to an external vibrationally isolated optical table via rods passing through flexible vacuum bellows. The 743 μm wavelength probe radiation is produced using an optically pumped far-infrared laser fixed on the table. A rotating grating wheel with a grating constant that varies periodically and continuously around the wheel circumference has been used to effect a smooth spatial scan of the plasma. This replaces a stepped grating wheel that was used previously.[3] The use of a continuously varying groove constant increases the duty cycle by reducing the number of transitions in the grating constant which can cause loss of signal. Using this grating, the probe beam has a full width at half maximum of 2 cm at the plasma center.

Recently, the air turbine grating drive was replaced with an electric motor to provide a stable computer controlled rotational speed and to make the system acoustically quieter. Nevertheless, the interferometer uses one beam polarization component to probe the plasma and the other as a vibration monitor to compensate for wheel induced vibrations. With the grating wheel rotating at 6000 rpm, and using a wheel with six grating periods (or partitions), a single scan of the plasma can be performed in 2 ms.

Signals are detected using corner-cube Schottky diode detectors. The signals are amplified and digitized directly, and the phase demodulation is performed numerically post-shot. The continuously sampled phase projection $\phi(p)$, where p is the impact parameter, is binned into a preset number of spatial channels $\phi_i(t)$, $i=1, \ldots, N$, chosen to obtain a satisfactory trade-off between spatial resolution and signal to noise ratio. We typically choose $N=30$. A Fourier shifting algorithm is used to correct for the nonsimultaneous spatial sampling due to the scanning nature of the interferometer. The discretized projections are stored in the MDSPLUS[5] data base and can be used to study the dynamics of a particular shot by either examining moments of the projection, as shown in Sec. III A or performing an Abel inversion to obtain the electron-density profile as shown in Sec. III B. To maximize the signal-to-noise ratio for these studies we have restricted the interferometer operation to the top-launched diagonal view of the plasma only. This achieves rms phase

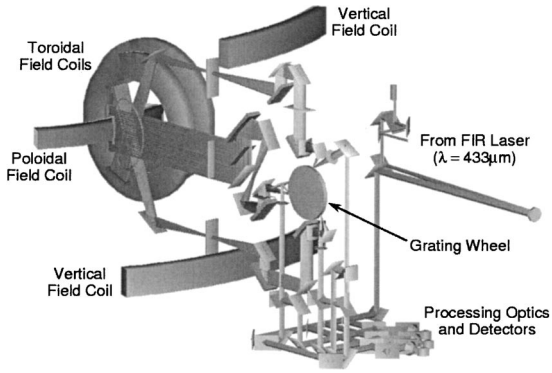

FIG. 1. Ray trace of the interferometer system produced using the GRT3D ray trace code (see Ref. 4).

[a]Electronic mail: scott.collis@anu.edu.au

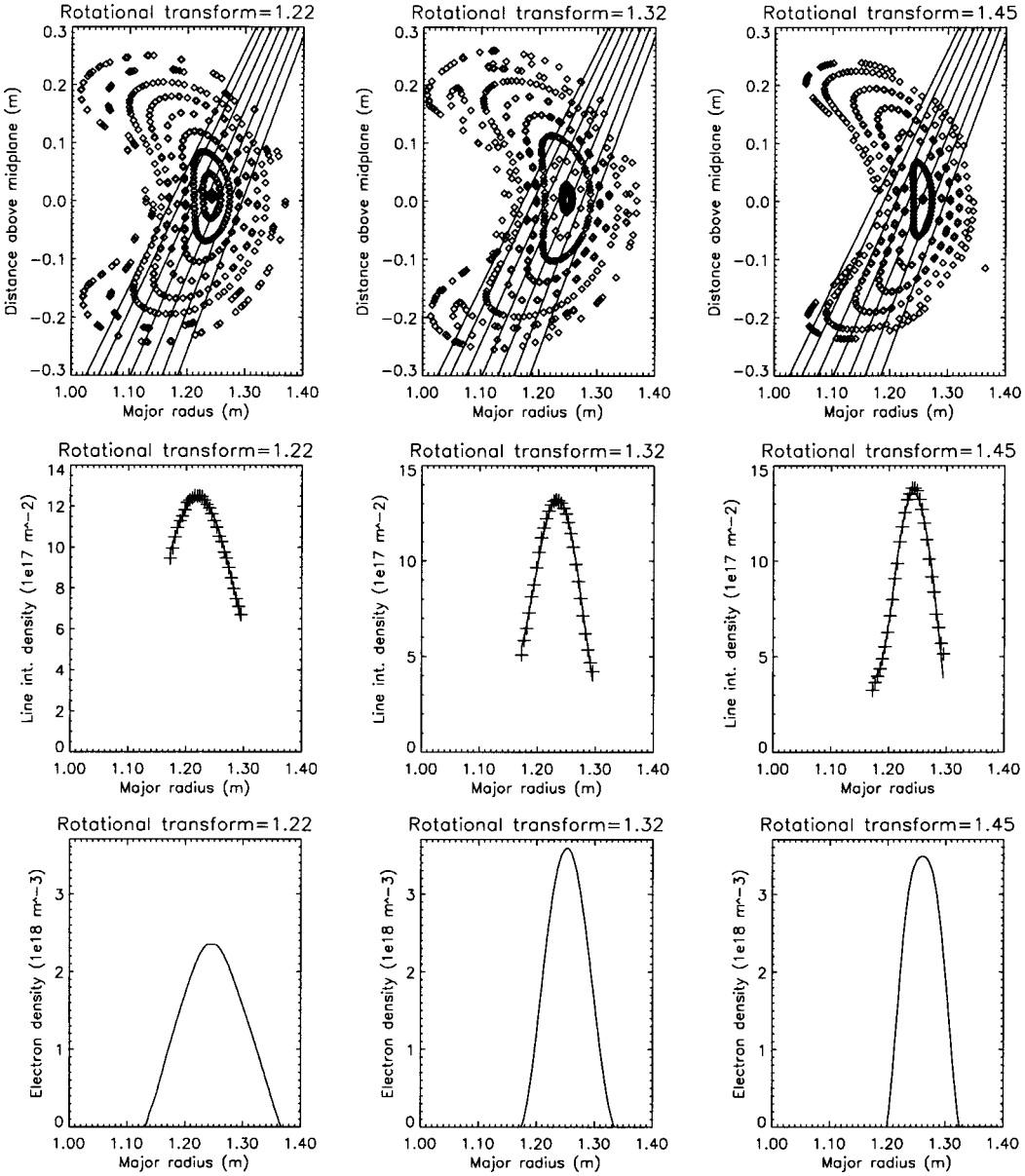

FIG. 2. Variation with the magnetic configuration (left to right) of the viewing geometry (top), projections shown as crosses and the best fit as a solid line (center), and reconstructions of the density profile (bottom).

noise levels of around 0.01 radians compared to a plasma induced phase shift of up to 3.5 rad. Figure 2 shows Poincaré plots of the magnetic surfaces for on-axis rotational transforms of 1.22, 1.32, and 1.45 and illustrates the interferometer spatial coverage with changing magnetic configuration. Also shown are representative snapshots of the density projections (crosses), their functional best fit, and the inverted density profile as a function of major radius.

III. PLASMA STUDIES

A. Profile effects under resonant heating

Mixtures of hydrogen and helium, in the ratio 2:1, were ionized and heated using 80 kW of power at the fundamental ion cyclotron frequency of 7 MHz at 0.46 T. Diamagnetic signals and spectroscopy results point to the plasma being colder than 40 eV. Results presented in this section were obtained for an on-axis rotational transform of 1.12 for which resonant conditions are obtained within the plasma cross section at on-axis fields between 0.44 and 0.54 T.

The three lowest-order moments of the projection give a convenient and quick measure of the global properties of the plasma profile

$$\mu^{(0)}=\sum_{i=1}^{N}\phi_i, \tag{1}$$

$$\mu^{(1)}=\frac{1}{\mu^{(0)}}\sum_{i=1}^{N}\phi_i x_i, \tag{2}$$

$$\mu^{(2)}=\frac{1}{\mu^{(0)}}\sum_{i=1}^{N}\phi_i (x_i-\mu^{(1)})^2. \tag{3}$$

Figure 3(a) shows the zeroth spatial moment of the projection, [Eq. (1)], at the time the plasma obtains its maximum density, versus the on-axis magnetic field. Figure 3(b) shows the second central moment of the projection, [Eq. (3)], which is related to the profile width, versus the on-axis magnetic

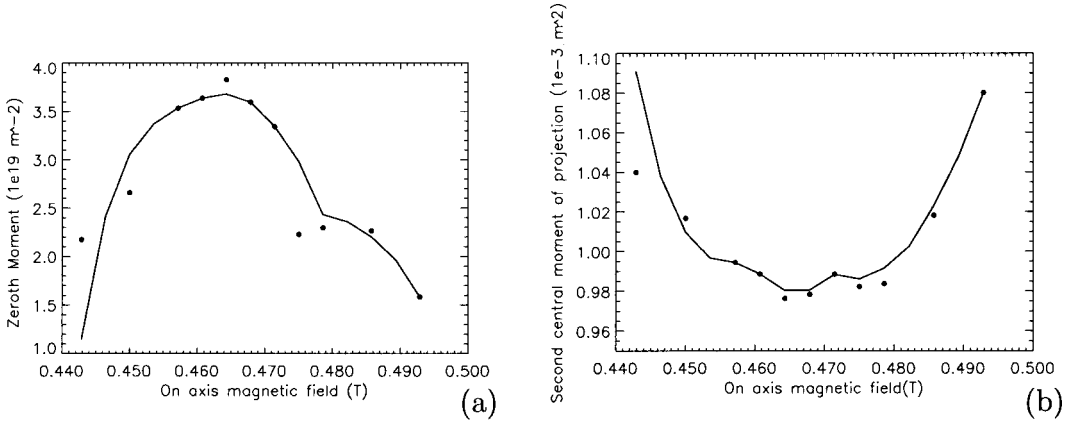

FIG. 3. (a) The zeroth and (b) second central moments of the projection as a function of on-axis magnetic-field strength. The fundamental resonant magnetic field strength for hydrogen ion cyclotron resonant heating at 7 MHz is 0.46 T.

field. The figures indicate that the number of electrons decrease and the profile broadens when the resonant layer moves away from the center of the plasma. This dependence of maximum density on the magnetic field is indicative of localized plasma production occurring at the resonant layer. It is reasonable to expect that when plasma production is displaced from the magnetic axis particles are more readily lost.

B. Magnetic configuration studies

We have used the interferometer to investigate the dependence of the plasma density profile on rotational transform. The ratio of central and helical coil currents have been varied to obtain on-axis rotational transforms ranging from 1.18 to 1.45. Figure 4(a) shows the projections, at the time of maximum density, versus the on-axis rotational transform. The solid line shows the computed position of the magnetic axis as a function of rotational transform. The peak of the projection follows, but does not precisely conform to the magnetic axis as both the position and shape of the profile contribute to the peak position of the projection.

The data shows plasma formation being inhibited when the 4/3 and 7/5 rational surfaces are present at the edge of the plasma. The 7/5 surface affects formation over a larger range of rotational transforms (1.35–1.37) due to the rational surface moving inwards at the same rate as the last closed flux surface moves inwards, i.e., the 7/5 rational surface exists at the edge of the plasma for a wide range of values of rotational transform. The 7/5 surface does not separate from the last closed flux surface until the on-axis rotational transform approaches 1.37.

Figure 4(b) shows the Abel inverted density profile, and Fig. 4(c) shows the number of electrons in the interferometer poloidal cross section as a function of the on-axis rotational transform. The rotational transforms at which we observe the highest densities correspond to the lower-order rationals (5/4, 4/3, and 7/5, respectively) moving away from the edge to the center of the plasma. The Abel procedure assumes that the density is constant on a flux surface and can be expressed as a linear combination of Bessel functions in magnetic flux coordinates. Negative density artifacts can sometimes be seen at higher-rotational transforms due to the limited interferometer spatial coverage of the plasma. We obtain an approximation to the flux surface coordinates for a variety of magnetic configurations by interpolating field line tracing results from the Gourdon code.[6] The projection is inverted by fitting the three lowest-order J_0 bessel functions in the image space. We have found that three terms are sufficient to give an adequate fit to the projections. A useful measure of the fidelity of the fit is the normalized residual

$$\epsilon = \sum_i \sqrt{\left(\frac{\phi_i}{\Sigma_j \phi_j} - \frac{f_i}{\Sigma_j f_j} \right)^2}, \tag{4}$$

where f_i is the best-fit phase shift. Figure 4(c) shows the number of electrons in the interferometer poloidal cross section as a function of on-axis rotational transform while Fig. 4(d) shows that ϵ remains relatively constant and below 0.04.

C. Abel symmetry violation

The reconstructions are obtained under the assumption that the density remains constant on a flux surface. Figure 5(a) shows a time series for a 0.5 T helium-hydrogen discharge where the plasma undergoes a reorganization that shifts the first moment of the projection by over 5% of the plasma radius. Figure 5(b) shows the time evolution of the first moment $\mu^{(1)}$ which shows two events at 40 and 65 ms giving rise to changes in the plasma density distribution. Because of the truncated view of the plasma, the center of mass cannot be used to unambiguously distinguish between significant but symmetric profile changes or departures from radial symmetry. Figure 5(c) shows the normalized residuals ϵ as a function of time. The event at 40 ms does not give rise to a sustained increase in the residual error, indicating that the plasma density remains constant on a flux surface. By contrast, the event at 65 ms gives rise to a significant and prolonged departure from Abel symmetry. To check the validity of the Abel inverted data we have reprojected the density profile along the line of sight of a 2 mm swept frequency interferometer, shown as the dashed line in Fig. 5(d). The two independent measurements of the projection show satisfactory agreement. However, neither the reprojected data, or the 2 mm signal (shown as a solid line), which views through the center of the plasma, detect the perturbation. This points to the perturbation having an odd symmetry.

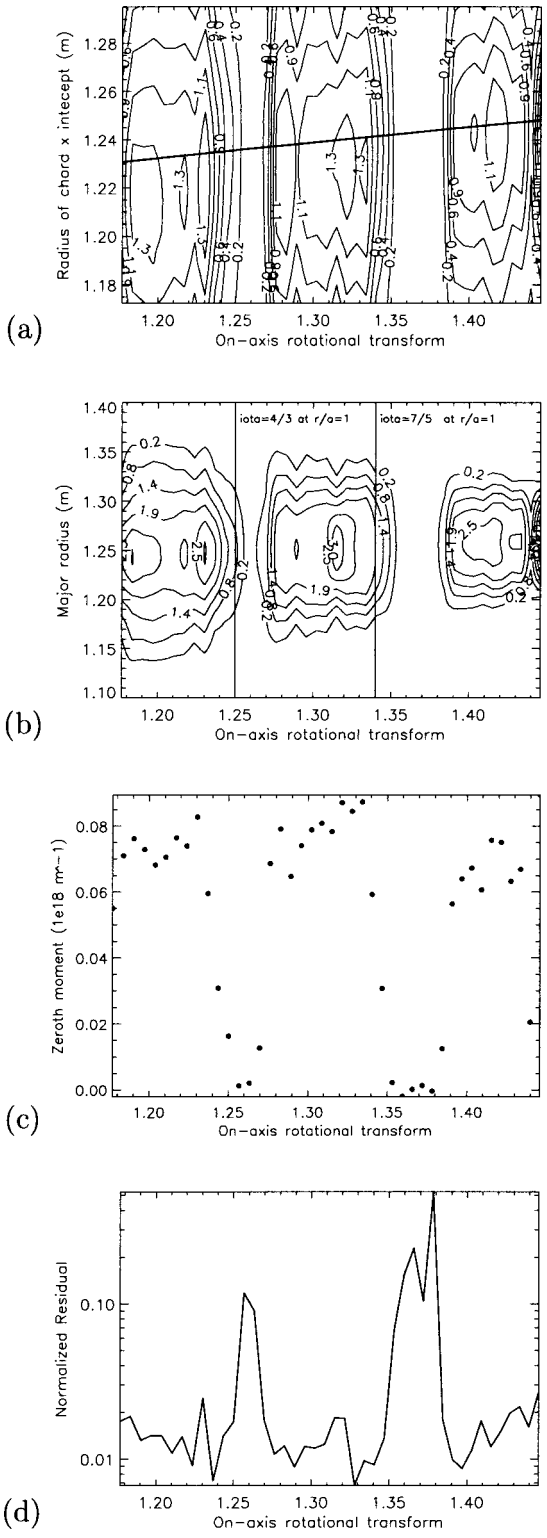

FIG. 4. Variation with on-axis rotational transform of the (a) projection of the density profile at maximum density, (b) inverted density profile, (c) the integrated electron density in the cross section of the interferometer, and (d) the normalized residual ϵ. These figures show that plasma formation is suppressed while low-order rational surfaces are present at the plasma edge.

IV. CONCLUSIONS

The H-1NF interferometer provides high-quality projections of the electron-density profile. Moments of the projections can give a quick indication of the plasma position and shape without recourse to symmetry assumptions. However,

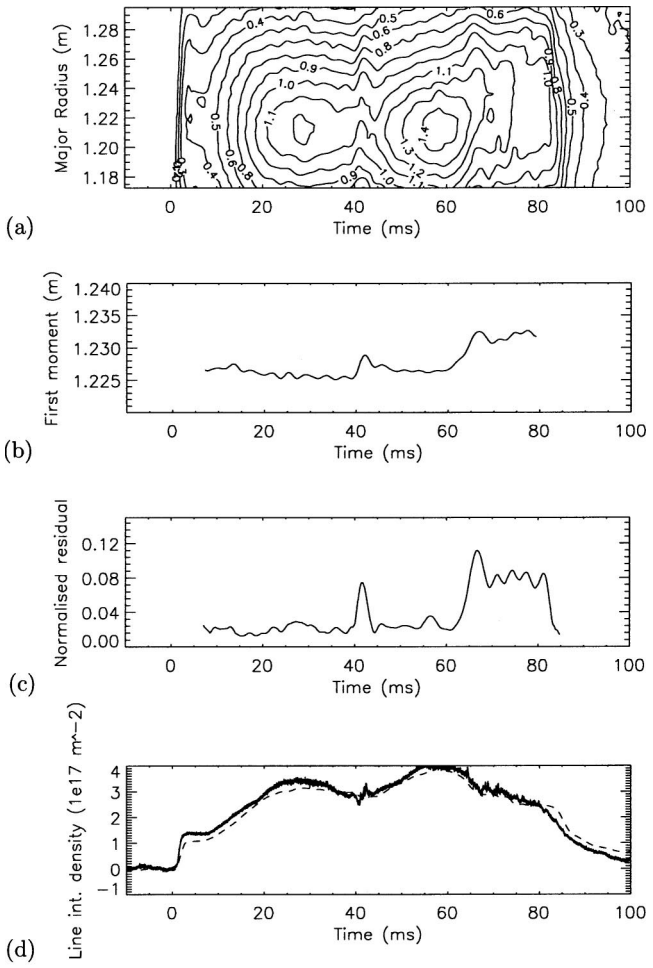

FIG. 5. (a) The projection of the density profile as a function of time for a discharge exhibiting a pronounced and sustained departure from Abel symmetry. The remaining figures show (b) the first moment of the projection, (c) a comparison between the line integrated electron density as measured by the two millimeter interferometer and that which would be measured based on the projections shown in (a) (Ref. 7).

by assuming that density is constant on a flux surface an Abel inversion can be performed to obtain the plasma density distribution. In this article, we have presented examples where the interferometer has been used to study H-1 plasmas. We have studied the effect of shifting the ion cyclotron resonant layer on the projection shape. The assumption of Abel symmetry is valid across a wide variety of configurations. This indicates that the plasma conforms closely to the computed flux surfaces. However, we have also presented data showing a substantial and sustained violation of this condition.

[1] S. Hamberger, B. Blackwell, L. Sharp, and D. Shenton, Fusion Technol. **17**, 123–130 (1990).
[2] J. Howard, Rev. Sci. Instrum. **61**, 1086 (1990).
[3] G. Warr, J. Howard, and L. E. Sharp, Fusion Eng. Des. **34–35**, 387 (1997).
[4] G. Warr and J. Howard, Rev. Sci. Instrum. **72**, 2305 (2001).
[5] J. A. Stillerman, T. W. Fredian, K. Klare, and G. Manduchi, Rev. Sci. Instrum. **68**, 939 (1997).
[6] C. Gourdon, D. Marty, E. K. Mashke, and J. Touche, Nucl. Fusion **11**, 161 (1971).
[7] D. Pretty, B. Blackwell, J. Harris, S. Collis, and J. Howard, Plasma Phys. Controlled Fusion (to be published).